Elsevier Editorial System(tm) for Earth and Planetary Science Letters
Manuscript Draft

Manuscript Number: EPSL-D-10-01094R2

Title: Denudation of the Namche Barwa Antiform, Eastern Himalaya

Article Type: Regular Article

Keywords: Himalaya; Tsangpo River; Siang River; fission-track dating; detrital zircon; thermochronology, numerical modeling

Corresponding Author: Dr. Eva Enkelmann, Ph.D.

Corresponding Author's Institution: University of Tuebingen

First Author: Eva Enkelmann, Ph.D.

Order of Authors: Eva Enkelmann, Ph.D.; Todd A Ehlers; Peter K Zeitler; Bernard Hallet

Abstract: The Namche Barwa massif has long been identified as a region of highly localized rapid exhumation. Previous studies suggest that this region contributes ~50% of the total sediment load of the Brahmaputra River, which cuts through the eastern end of the high Himalayan Range and exits into the Indian plain. This study presents new detrital zircon cooling ages from 19 sand samples collected along the Brahmaputra River and tributaries with catchments covering the Namche Barwa massif, and its surroundings, including the so-far unexplored regions in the south. The new results confirm that the Namche Barwa massif is a major source of sediment for the Brahmaputra River composing 60-70% of the entire load. Furthermore, the data from southern regions much better constrains the extent of young cooling ages at Namche Barwa, modestly extending this zone to the south. Our more robust and higher estimates of sediment yield from Namche Barwa together with the increased source area give decadal timescale denudation rates of 8 - 12 mm/yr. Results from thermokinematic modeling of the ages suggest million-year timescale denudation rates as high as 7-9 mm/yr.

Denudation of the Namche Barwa Antiform, Eastern Himalaya

Enkelmann, E.[1]*, Ehlers, T.A.[1], Zeitler P.K.[2], Hallet, B.[3]

1) Department of Geoscience, Universität Tübingen, Wilhelmstr. 56, 72074 Tübingen, Germany, eva.enkelmann@uni-tuebingen.de, todd.ehlers@uni-tuebingen.de, phone: +49 7071 2973151

2) Earth and Environmental Science Department, Lehigh University, 1 West Packer Avenue, Bethlehem, PA 18015-3001, USA, peter.zeitler@lehigh.edu, phone: +1 610 758 3671

3) Department of Earth and Space Sciences, University of Washington, 4000 15th Avenue NE Seattle, WA 98195-1310, USA, hallet@u.washington.edu, phone: +1 206 543 0489

* corresponding author

Abstract

The Namche Barwa massif has long been identified as a region of highly localized rapid exhumation. Previous studies suggest that this region contributes ~50% of the total sediment load of the Brahmaputra River, which cuts through the eastern end of the high Himalayan Range and exits into the Indian plain. This study presents new detrital zircon cooling ages from 19 sand samples collected along the Brahmaputra River and tributaries with catchments covering the Namche Barwa massif, and its surroundings, including the so-far unexplored regions in the south. The new results confirm that the Namche Barwa massif is a major source of sediment for the Brahmaputra River composing 60-70% of the entire load. Furthermore, the data from southern regions much better constrains the extent of young cooling ages at Namche Barwa, modestly extending this zone to the south. Our more robust and higher estimates of sediment yield from Namche Barwa together with the increased source area give decadal timescale denudation rates of 8 – 12 mm/yr. Results from thermokinematic modeling of the ages suggest million-year timescale denudation rates as high as 7-9 mm/yr.

Keywords: Himalaya, Tsangpo River, Brahmaputra River, fission-track dating, detrital zircon, thermochronology, numerical modeling

1. Introduction

One of the most impressive features in the Himalaya-Tibet orogen is the Namche Barwa–Gyala Peri (NB-GP) massif (Figs. 1 and 2). The massif contains a crustal-scale north-plunging antiform that exposes high-grade metamorphic rocks of Indian basement origin (Fig. 1). Some of the most extreme relief (~7 km over 40 km window) on Earth is found at the northern tip of the antiform where the Brahmaputra River makes a 180° turn and cuts through the high peaks with exceptional energy (e.g. Finlayson et al., 2002; Finnegan et al., 2008,). Because of the tremendous size of the Brahmaputra drainage basin the discharge of the river is much higher than that of other rivers crossing the Himalaya. This massive discharge combines with the steep descent of the river to give it exceptional potential to erode bedrock. Previous thermochronometric studies of the bedrock have documented extremely rapid and spatially localized long-term exhumation rates (3-5 mm/yr over ~10^6 yr, Fig. 2; e.g. Burg et al., 1998; Seward and Burg, 2008; Booth et al., 2009). Furthermore, rapid modern rates of erosion inferred from the rate of energy release in the river are spatially coincident with the locus of long-term exhumation and exposures of high-grade metamorphic rocks (Finlayson et al., 2002; Finnegan et al., 2008). Although limited in spatial extent, the rapidly exhuming region is thought to have had a large impact on the sediment load in the Brahmaputra river network (e.g. Singh and France-Lanord, 2002; Garzanti et al., 2004). For example, when the Brahmaputra River exits the Himalayan Range about 50% of the sediment load originates from the NB-GP massif, an area that makes up only 2% of the entire catchment (Fig. 1; Stewart et al., 2008). This large sediment flux from a highly localized region has significant implications for studies of synorogenic sedimentation and studies that treat the detrital record as an archive of hinterland processes. Note that in our discussions we distinguish at times between the larger scale Namche Barwa antiform and the smaller NB-GP metamorphic massif active at the northern end of the antiform (Fig. 1).

We confirm previous work and much more tightly constrain in the extent of the rapidly exhuming region by presenting new detrital zircon fission-track (zFT) cooling ages from 19 samples of the Brahmaputra River and tributaries whose watersheds cover the area of the entire NB-GP antiform and surrounding areas (Figs. 1 and 3). These data provide the first detailed definition of mineral cooling ages for the region southwest of the NB-GP massif. (Figs. 2 and 3). Furthermore, we use the revised areal extent over which young cooling ages are found to quantify spatial variations in the modern (10^0 yr) fluvial sediment load and long-term (10^6 yr) erosion from the entire antiform and massif from thermokinematic modeling. Our larger data set indicates that rapid denudation extends further south (~50 km) than previously recognized, and that sediment from this massif makes up an even larger fraction of modern sediment load of the Brahmaputra River than previously reported.

2. Background

The Eastern Himalayan syntaxis (Fig. 1) forms a broad deflection in geomorphic, structural and tectonic trends in the crust at the eastern end of the Indian plate, where dip-slip thrust tectonics transition eastward to dominantly strike-slip faults (Koons, 1995; Hallet and Molnar, 2001). The peaks of Namche Barwa (7782 m) and Gyala Peri (7294 m), which define the eastern termination of the Himalayan Range, are separated by one of the world's deepest gorges that was incised by the Brahmaputra River (Fig. 1). This river transports sediments derived from much of the southeastern Tibetan Plateau and the northern side of the central and eastern Himalaya. As it plummets ~2500 m off the plateau it slices through the NB-GP massif along a steep reach where the rate of energy dissipation by the river is the highest in the entire Himalayan Range (Fig. 1; Finlayson et al., 2002). Within the NB-GP massif at the northern end of the Nanche Barwa antiform, petrological data and U-Pb dating of accessory minerals from high-grade basement rocks document exhumation from depths of ~40 km within the past 3 to 10 Ma, requiring mean exhumation rates of 4-8 mm/yr over this period (Booth et al., 2004, 2009; Burg et al., 1998). As would be expected under conditions of such rapid and prolonged exhumation, cooling ages measured from bedrock in the metamorphic massif are very young due to both the high exhumation rates and the steepening of the local geotherm (Craw et al., 2005). Biotite $^{40}Ar/^{39}Ar$ ages of < 2 Ma are confined to this massif as defined by its active boundaries in the form of steep brittle fault zones (yellow contour Fig. 2; Stewart et al., 2008). Zircon U-Th/He and zFT ages of < 2 Ma occur over a slightly larger region that includes rocks of the Asian-affinity Lhasa block in the NW (red contour, Fig. 2; Burg et al., 1998; Stewart et al., 2008; Seward and Burg, 2008).

Stewart et al. (2008) conducted FT and U-Pb dating of detrital zircons taken from two series of samples of Brahmaputra River sands, one taken immediately upstream of the metamorphic massif (location O, Fig. 1 and 3), and another taken well downstream at Pasighat, where the Brahmaputra River exits the Himalaya Range (Fig. 3). Based on the occurrence of a young age population that peaks at 0.6 Ma and makes up 47% of the entire measured zircon population (data shown in Figs. 3 and 4, Table 1) in the downstream sample they argued that the only possible source of these ages was from the NB-GP massif. Using the exposed area of young bedrock ages (Fig. 2), Stewart et al. (2008) calculated a modern-day aerially averaged exhumation rate of ca. 10 mm/yr for this region, based on the percentage of young zFT grains in the downstream sample and the measured sediment flux at Pasighat. The distinct young cooling age signal from the Namche Barwa area is not only preserved in the sediment load where the Brahmaputra River exits the Himalayan range, but also much farther downstream in the basin in Bangladesh. Zircon U-Th/He dating of sediments from the Brahmaputra Basin yielded 40% of grains with cooling ages that range between 0.4 and 1 Ma, with a peak age at 0.5 Ma that correspond closely to the corresponding bedrock cooling ages from the zone of rapid exhumation at Namche Barwa (Tibari et al., 2005). Another 40% of the grains range from 2.5 to 7 Ma corresponding to cooling ages from the drainages of the other Himalayan Rivers. Geochemical studies of modern sediment loads (Singh and France-Lanord, 2002) also suggest that denudation rates within the entire Brahmaputra catchment are spatially highly nonuniform and that the NB area sustains 45% of the total sediment flux of the Brahmaputra above its confluence with the Ganges River (Fig. 1).

3. Methods

Zircon FT thermochronology is well-suited for detrital exhumation studies because of the robustness and relative ubiquity of zircon, and the high closure temperature of 250±40 °C (Brandon et al., 1998). The closure temperature can be substantially higher (>300°C) if cooling rates are high and the zircons lack radiation damage (Tagami et al., 1998, Rahn et al., 2004). Alternative methods commonly used in active mountain belts include apatite U-Th/He and FT, which have lower closure temperatures (55-75°C and ~100-110°C, respectively; Farley, 2000; Schuster et al., 2006; Green et al., 1986; Carlson et al., 1999). The lower closure temperature of the apatite systems means that apatite U-Th/He or FT ages will only record processes involving the uppermost ~0.5 to 4 km of the crust depending on the geothermal gradient. Thus in areas of high relief in active mountain belts, apatite data are as likely to record denudation processes related to transient landscape evolution as processes related to more persistent and longterm exhumation of bedrock from significant depths of 5 to 15 km (Mancktelow and Graseman, 1997). Accordingly, one could argue that data from higher closure temperature systems are more valuable as a measure of "geodynamically significant" exhumation that perturbs thermal gradients, advects rocks from crustal depths much greater than the local relief, and is longer-lasting. Thus, the presence of a Pleistocene zircon FT age population suggests that rapid exhumation and rock uplift have been sustained long enough to remove 5 to 15 km of crustal material, whereas apatite cooling ages of a similar age might merely reflect glacial carving of the landscape during the Quaternary.

Here we report 1423 new detrital zFT ages from 15 modern rivers whose catchments cover most of the NB-GP massif and the surrounding region (Figs. 1 and 3). We combine these analyses with 187 zFT ages of four additional samples published by Stewart et al., (2008) (samples A, C, F and O, Fig. 3). The catchments sizes for our samples vary from 12 to 260,000 km^2; samples from the larger rivers encompass the sediment source area for the entire Brahmaputra River, whereas smaller tributary catchments provide a more focused look at sediment source (Figs. 1 and 3; Table 1). During our sampling of tributaries we were careful to sample at locations unaffected by sediments transported from the Brahmaputra up the tributaries (i.e. backflow) during high discharge events such as floods or the Monsoon.

Sediment deposited from backflow was easily identified in the lower part of the Brahmaputra River where relief is lower. In these backflow influence areas we sampled further upstream of the tributary-trunk confluence to avoid contamination from backflow (e.g. sample M).

Detrital zircons were separated from medium- to coarse-grained sand using standard magnetic and heavy liquid techniques. Zircon FT ages were measured at Union College following procedures described by Garver and Kamp (2002) and Garver (2003). We prepared 3 to 4 zircon mounts per sample. The polished mounts were etched for 15 to 30 hours in a KOH:NaOH eutectic solution at 228°C to reveal fossil tracks. Zircon mounts where then covered with a uranium-free muscovite external detector and irradiated with thermal neutrons utilizing the nuclear reactor at Oregon State University. The neutron irradiation produced induced fission tracks that were revealed in the external detectors by etching in 48% HF at room temperature for 18 minutes. Tracks were counted using an automated stage and Olympus BH2 microscope at 1250x magnification.

At least 100 single grain ages were measured per sample, except for three samples that had an insufficient yield of zircons during mineral separation. Distributions of grain age from each catchment were analyzed using a grain-age-deconvolution and binomial peak-fitting procedure (Galbraith and Green, 1990; Brandon, 1992, 1996) to determine statistically significant populations of cooling ages. In Table 1 we give the results of the peak fitting procedure, but all single grain data for each sample are given in the supplement data repository.

4. Observed Cooling Age Distributions

The statistically significant catchment-average age populations and peak ages identified for each measured cooling-age distribution are summarized in Table 1 and shown as pie charts and probability density plots in Figures 3 and 4, respectively. Overall we find eight age populations that ranged from ~55 to <1 Ma (Table 1). In the following we divide the observed age populations in old (> 18 Ma) and young (<11 Ma) populations based on published cooling ages that suggest a Late Miocene onset of faulting and exhumation in the Namche Barwa antiform (see also discussion; e.g. Ding et al., 2001; Zhang et al., 2004). The older (>18 Ma) age populations represent ages that are often recognized in the wider Himalaya–Tibet region and do not reflect the evolution of the antiform itself. The observed spatial distribution of old and young populations is described next.

The older cooling age populations in the data set with peak ages between 55 to 18 Ma (P8-P5; Table 1) occur mostly in distal drainages surrounding the NB-GP antiform (grey colored in pie charts of Fig. 3). The percentage of these older cooling ages increases with increasing distance from the NB-GP massif. Such cooling ages make up as much as ~70 % of the entire age distribution in the Brahmaputra sample upstream of the river gorge (sample O), but only <20% of the age distribution in the samples immediately downstream of the NB-GP massif (sample Q and R), and ~100 km further where the river exits the Himalayan Range (sample S and Pasighat sample 301 of Stewart et al. (2008); Fig. 3).

Several young cooling age populations occurring in differing proportions in samples from various parts of the region (e.g. P1-P4; Fig. 3) reflect the more recent exhumation history of the NB-GP antiform. Whereas, the 11±1 Ma (P4) and 7±1 Ma (P3) cooling-age populations occur in drainages proximal to the NB-GP massif (samples B-F, J, K and M), the younger age populations at 3.5±1 (P2) and 0.9±0.6 Ma (P1) occur only within the antiform (sample H, I and J), and P2 in areas north of the northwestern flank (samples D, E and F). The two samples from the Brahmaputra River collected downstream of the area of most rapid exhumation (sample R and S) both yielded a young cooling age population with a peak at ca. 1 Ma and that comprises 61-70% of the entire sample (Table 1). This high percentage of the <1 Ma peak suggests that these young zFT grains originated from the rapidly exhuming NB-GP massif. These values are apparently higher than the suggested 47% of the youngest age population found in the Pasighat sample (301) by Stewart et al. (2008). However, comparing the measured grain age distribution of the 301 sample with our sample at Pasighat (S) reveals that they are similar (Fig. 4) with single grain ages ranging from 0.1 to 50 Ma (sample 301) and 0.2 to 56 Ma (sample S; Table 1). The difference in the size of the youngest age population can be explained two ways: (1) Reviewing the single grain measurements of Stewart et al., (2008) reveals that no 0-track grains were measured, however, such grains most probably existed, as many grains had only one fossil track, and several 0-track grains were measured in our samples. Avoiding those 0-track grains for analysis leads to an underestimation of the number of young grains, and consequently the size of the youngest age population with respect to the other age populations. (2) The binomial peak fitting procedure is sensitive to small changes in the measured age distribution. In contrast to our Pasighat sample S where the binomial peak fitting procedure yielded only one young age population (P1=0.9 Ma, 61%), it yielded two peaks (P1=0.6 Ma, 47% and P2=4.7 Ma, 13%) in Pasighat sample 301, which together make up 60% of the entire sample. To compare the two Pasighat samples we excluded the 0-track grains of our sample (S) and compared the cumulative distribution function with Stewart's sample (301). A two-sample KS statistical test does not allow concluding that the two samples are from different populations.

Detrital cooling ages from small (<1500 km^2) catchments on the flanks of the NB-GP antiform provide significant additional constraints on the lateral extent of rapid denudation (Fig. 3). On the northwestern flank, samples show small fractions of moderately young ages (~3.5 Ma peak) and none less than 1 Ma. This suggests that in this region, the cooling age contours inferred by Stewart et al. (2008) from bedrock cooling ages are robust (red contour; Fig. 2). To the southeast of the antiform, there is a sharp difference in youngest peak cooling ages from catchments located on either side of the Brahmaputra (sample I and K; Fig. 3).

5. Discussion

The spatial variations in cooling ages have several implications for the exhumation history of this region. Here we discuss: (1) how the older and younger zFT peaks are representative of spatial variations in the sediment sourced from outside and within the massif, respectively, (2) a large and spatially variable discontinuity in cooling ages across the structurally bounded flanks of the antiform, (3) how previous estimates of the modern (10^0 yr) sediment flux from the antiform to the Brahmaputra river system are underestimates, and (4) spatial variations in long-term (~10^6 yr) denudation rates estimated from a 1D inverse model.

5.1 Spatial variations in the sediment source

The large difference in the cooling-age distribution of the Brahmaputra River upstream and downstream of the gorge reflects a substantial contribution of sediments from the rapidly exhuming rocks of the massif. The older ages are clearly related to the earlier collision and denudation history of the region documented by others (e.g. Yin and Harrison, 2000 and references therein) whereas young cooling ages located within the massif itself represent rapid exhumation of the massif over the last 10 Ma. The P3 and P4 peaks are generally consistent with previous work related to the timing of initial deformation and exhumation in the present-day antiform. Based on bedrock thermochronology a later start at ~4 Ma was suggested for the northeastward transgressive growth of the NB-GP antiform into Asian crust (Seward and Burg, 2008). Biotite, muscovite, and hornblende $^{40}Ar/^{39}Ar$ ages from mylonites of the northwestern flank of the NB-GP antiform were dated at 8-6 Ma and also interpreted to date the beginning of faulting due to rapid uplift of the antiform (Ding et al., 2001; Zhang et al., 2004). The best constraint on timing comes from geochronological and petrological studies on high-grade metamorphic rocks (Booth et al., 2004, 2009), which suggest ~11-10 Ma as the beginning of metamorphism and anatexis at the NB-GP massif, with rapid decompression being underway by 6 Ma or well before. Late Miocene (< 11 Ma) zFT cooling ages occur in all samples with drainages that cover at least parts of the NB-GP antiform (I,J,M) and the area to the north along the active Jiali transform fault (B,C,D,E,F). This spatial distribution supports the suggestion that faulting at the flanks of the antiform and the transition zone to the Jiali fault is ongoing since the Late Miocene (Fig. 3). In the NB-GP massif itself, these Late Miocene cooling ages do not occur in the detrital or bedrock samples. Only younger (Pliocene to Pleistocene) cooling ages are observed and highlight the much higher rates and amounts of exhumation in this area (Figs. 2 and 3).

The spatial pattern of the youngest (<3.5 Ma) cooling-age populations suggests that the area of exposed young cooling ages is more extensive than previously thought (Fig. 2). Young (< 3.5–1 Ma) zFT cooling ages are prevalent in the age distributions in catchments located in the southern part of the antiform (samples J and I). Although the detrital data lack tight spatial resolution, they suggest that there is a region of exhumation at least sufficient to expose young zFT ages that extends ~50 km further south and southwest of the NB-GP massif. This region is located on the southeast side of the drainage divide that is coincident with the axis of the antiform (red contour, Fig. 3).

An alternative interpretation of the young cooling ages from the massif is that these samples could record the cooling age of young plutons intruded at shallow depths. This interpretation can be excluded, however, because (1) although dikes of <10 Ma occur in the NB-GP massif, they are volumetrically insignificant and so far have only been found within the metamorphic massif (Booth et al., 2004), and (2) U/Pb dating of detrital zircons from the Brahmaputra River shows no zircon U-Pb ages of < 10 Ma (a quarter of the zircon population gives ages ranging from 70-40 Ma, typical for the Gangdese belt batholiths (Lhasa block), and the majority of grains giving ages of 400-3000 Ma, typical for the Pan-African and Late Proterozoic basement of the NB-GP antiform (Stewart et al., 2008; Cina et al., 2009).

5.2 Structural controls on spatial variations in cooling ages

A significant additional constraint on the lateral extent and structural control of the rapidly exhuming region is evident from the contrast between youngest age populations found in catchments in and around the antiform (Figs. 3 and 4). There is a sharp difference in the youngest cooling age peaks found in catchments located on either side of the Brahmaputra River (1.6 Ma vs. 13 Ma in sample I and K, respectively). This difference reflects a large spatial gradient in exhumation rate, and suggests that the southeastern part of the antiform accommodated vertial displacement of several kilometers, whereas south of the anticline significant slower exhumation occurred since the late Miocene (Fig. 3). This difference in cooling ages would be consistent with active uplift and localized deformation or faulting on the SE flank of the antiform, however, the geology and structures of this region have not been mapped in detail.

5.3 Estimate of modern day denudation rates

The relative (percent) contributions of different cooling age peaks along the Brahmaputra river network can be integrated with modern sediment flux data to quantify the fraction of sediment derived from within, or outside of the massif. This approach assumes that the zircon concentration in the granitoides and gneisses that dominate the bedrock of the antiform and also in the sediments are broadly uniform. This assumption is supported by the fact that the zircon concentration in the various sand samples from the Brahmaputra and all the tributaries are similar.

Stewart et al. (2008) presented an approach to calculate the modern denudation rates in the NB-GP massif, which we will shortly review here: The annual suspended sediment load at Pasighat is estimated to be ~210 Mt, based on nine years of direct measurements of suspended sediments in the Brahmaputra at Pasighat from 1971 to 1979 (Goswami, 1985). More extensive measurements of sediment flux have been done further downstream between 1955 and 1972 (Goswami, 1985), as well as geochemical studies that reflect sediment provenance (Singh and France-Lanord, 2002). Together all these studies suggest an annual sediment load of 233 ± 92 Mt at Pasighat (Stewart et al., 2008). Stewart et al., (2008) used the relative abundance of 46% of detrital zircons at Pasighat that originate from the NB-GP massif (this number is the average of the population determined by zFT analysis (47%) and zircon U/Pb analysis (45%)) to estimate the modern denudation rate of the source area. They used the portion of 46% of the annual 210 ± 92 Mt sediment load instead of the 233 ± 92 Mt range mentioned above to get a conservative estimate of denudation rate. They converted the annual sediment load to an equivalent volume of bedrock eroded annually using a bedrock density of 2850 kg m^{-3}. They estimated that 3.4 x 10^7 m^3 of bedrock was eroded annually from the region exhuming rapidly; this volume could range widely due to the range of estimates for the sediment load. The spatial distribution of bedrock cooling data were then used to estimate the size of the area producing zFT cooling ages younger than ca. 2 Ma (Stewart et al., 2008). The closure temperature of zircon FT lies between those of zircon U-Th/He and biotite $^{40}Ar/^{39}Ar$ (180-200°C and 350-400°C, respectively; e.g. Reiners et al., 2004; McDougall and Harrison,1999) contour lines in Fig. 2). An average area of 3300 ± 550 km^2 was used as the best estimate for the area of exposed zircons with FT ages of less than 2 Ma (Stewart et al., 2008). Using these estimates of the volume of bedrock eroded annually and the size of the rapidly eroding area, they constrained the modern denudation rate averaged over the NB-GP massif to be between 7 and 21 mm/yr (Stewart et al., 2008). This denudation rate represents the denudation rate over the last few decades for which sparse discharge and sediment concentration are available for the eastern reach of the Brahmaputra.

Our new results suggest two modifications to this previous estimate of modern denudation rate by Stewart et al., 2008). First, we extend the region of very young, <2 Ma cooling ages to the south of the Namche Barwa antiform, at least 50 km southwest from the previous known locus of young ages. This band of young ages increases the inferred source area for young zFT ages by ~1500 km^2, with the new total area of 4800 ± 550 km^2 (red contour, Fig. 3). Second, we take into account our finding that the proportion of the Pasighat sediment load making up the young zFT age population, peaking at ~1 Ma, is larger than previously reported: 61 and 70% (samples S and R) compared to ~47% reported by Stewart et al. (2008). Note that sample R in particular more tightly constrains the magnitude of sediment contributed from Namce Barwa because it is located upstream, closer to the location of the antiform and thus less prone to dilution by older ages sourced from the foothills (e.g. catchments L, M, N). However, the Pasighat sample is most appropriate to use for denudation calculations because it has the associated sediment-load data. Taking 61 to 70% of the estimated modern annual sediment load, 210 ± 92 Mt we calculate that between 72-212 Mt/yr of sediment as sourced from the region of young zFT ages. Using a bedrock density of 2850 kg/m^3 the previous sediment load can be converted to an annual eroded bedrock equivalent of 2.5 to 7.4 x 10^7 m^3. Distributing this volume of bedrock over the 4800 ± 550 km^2 source area of young ages leads to an estimate of the annual denudation rate of 10 mm/yr for the NB-GP massif, but the estimates range widely from 5 to 17 mm/yr. This new estimate for the average modern denudation rate of the massif is identical to that reported by Stewart et al. (2008) for a smaller geographic area. Our new cooling ages representing a broader area (1) indicate the region over which rapid exhumation occurs is ~45% larger than previously thought, which increases the source area from previous estimates of 2% to a new value of 3% of the entire Brahmaputra drainage, (2) the proportion of the suspended sediment load of the Brahmaputra is also increased substantially, from 33 to 52%, and (3) the previous two results offset each other to produce a modern denudation rates in the antiform identical to that estimated previously.

5.4 Estimate of long-term denudation rates

The modern denudation rate just discussed represent processes operating over a decade, a geological instant. We now consider the long-term (~10^6 yr) exhumation rates using an integration of the youngest peak ages in our samples with a 1D thermal-kinematic and erosion model. In the last few decades numerous approaches have emerged for quantifying long-term denudation rates from thermochronometer data (e.g. see Ehlers 2005 for a review). All approaches use thermal models of varying complexity to estimate the thermal structure the samples cool through. A detailed modeling study of our cooling ages is beyond the scope of this paper. Rather, we build upon previous work in the Himalaya (e.g. Whipp et al., 2007, 2009; Rahl et al. 2007) to estimate spatial variations in denudation rates from the mean and one standard deviation variation in the youngest measured peak ages. As demonstrated by Whipp et al., (2007, 2009) a 3D thermal model is often unnecessary for quantifying the catchment average denudation rates in rapid eroding regions, even for low closure temperatures less than ~300 °C. Whipp et al (2009) also document catchment scale processes such as changes in relief are typically unquantifiable in detrital grain age distributions, particularly when denudation rates are high. Given these natural limitations, we follow the approach of Rahl et al., (2006) and use a 1D transient thermal model to quantify the first-order variations in geologic denudation rates between catchments. Future work, with the addition of more bedrock and detrital data from other thermochronometer systems may warrant a more sophisticated analysis.

We calculate the range of denudation rates that could produce the youngest peak age in each catchment using a 1D Monte Carlo inverse model. The model uses the youngest peak age as input and then randomly selects a transient denudation rate, basal temperature, and thermophysical properties from a range of values described below. A transient denudation history model was used rather than a steady-state model because the onset time of denudation for each catchment is not known, nor is the variation in denudation rates during exhumation known. Both of these factors can have a large effect on the thermal field samples cool through. Because of this, we chose to treat the onset time of denudation and also the range of denudation rates during exhumation as free parameters in the transient model. A predicted zFT age is calculated from the transient thermal field calculated from a random selection of model parameters over the ranges specified below. A Chi-squared statistical misfit is calculated for each model using the predicted age, and the observed peak age with its one-sigma variability. The procedure was repeated 300,000 times to assure a completely random evaluation of all possible parameter combinations. Simulations with a Chi-squared misfit of 1 fit the data within the 1sigma observed variability and were deemed acceptable fits to the data for the prescribed denudation history and other parameters. The model used is from Whipp et al., (2009) modified for the previously described 1D Monte Carlo approach. Cooling rate dependent predicted zFT ages were calculated using the effective closure temperature concept and approach described in Ehlers et al. (2005).

The predicted range of denudation rates following sample closure are presented in Figure 5 for individual drainage areas of three different parts of the study area (the NB antiform, areas north and northwest of the antiform, and the drainages south of the antiform). Results are shown for hot (setup 1) and cold (setup 2) basal temperatures to demonstrate the maximum range of thermal fields that could fit each peak. The hot setup (1) has 875°C at 40 km (model thickness), a heat production of 3 μWm^{-3}, and a thermal conductivity of 3.5 $Wm^{-1}K^{-1}$. The cold setup (2) has a basal temperature of 800°C, a heat production of 1 μWm^{-3}, and a thermal conductivity of 2.5 $Wm^{-1}K^{-1}$. For both setups, denudation rates were randomly selected to vary between 0.05 to 10 mm/yr. Rates were held constant for time intervals of 2-16 Myr up to the maximum exhumation duration. The one-sigma uncertainty in peak ages is represented with (x-axis) error bars, and the range of possible denudation rates fitting each setup is also shown (y-axis) error bars. The previously described approach for calculating denudation rates is intentionally conservative and designed to report the complete range of denudation rates that can fit the observed peak age distributions given the model assumptions (1D transient) and range of parameters explored.

Predicted denudation rates are 0.6 ± 0.1 mm/yr at the western end of the NB antiform, and increase to >2 mm/yr in the south-central part of the antiform (Fig. 5). Denudation rates are exceptional high with ~8 ± 1 mm/yr at the NB-GP massif (Fig. 5). In contrast the areas northwest and south of the NB antiform show low denudation with rates of ~0.1 to 0.4 mm/yr south of the NB antiform, and in the north and northwestern area denudation rates are up to ~1 ± 0.2 mm/yr (Fig. 5).

The model results show that the long-term denudation rates, those integrated over a 10^5 to 10^6 year timescale, of the NB-GP massif are slightly lower (8.0±1.0 mm/yr) than the modern day denudation rates calculated from the annual sediment flux (10.0±2.0 mm/yr). The previous comparison of denudation rates over geologic and modern (sediment flux) time-scales is not, however, without pitfalls. It is well known from analysis of sedimentation rates (Saddler, 1983) that there is an inherent bias associated with the rate calculated and the time span the rate is calculated over. This bias also applies to calculation of denudation rates and is due to discontinuities or hiatuses in process considered. These discontinuities cause rates calculated over short time scales to be higher than those over long time scales (e.g. see discussion in Willenbring & von Blanckenburg, 2010). Given this limitation, the most reliable conclusions that can be reached from Figure 5 are that (a) spatial variations in denudation rates are present and highlight exceptionally high erosion rates in the NB antiform and in particular the NB-GP massif. These high rates exceed those found outside the antiformal structure; and (b) the rapidly denuding regions of the antiform are eroding over the last ~1 Ma at a rate similar to that suggested from our modern sediment flux calculation (~8-10 mm/yr).

6. Implications and Conclusions

The primary result from this study is documentation of the larger spatial area over which rapid exhumation occurs in the Namche Barwa antiform. Implications of this finding for understanding exhumation of the Himalaya-Tibetan orogen are as follows.

First, previous bedrock and detrital thermochronology studies documented rapid exhumation over the last ~10 Myr occurring in a relatively isolated region near the NB-GP massif. Here we find that the zone of young (< 2 Ma zircon FT) cooling ages extends ~50 km further southwest than previously thought. This zone of rapidly cooled rocks has a distinct signature in modern fluvial sediments measured along the Brahmaputra River.

Second, the observations of young zFT ages across an extensive portion of the NB antiform lead to two possible models for the evolution of this structure. One possibility is that over the last 10 Myr the location of rapid exhumation has been stationary and has narrowed and focused through time towards the Brahmaputra gorge. This model would be consistent with the 'tectonic aneurysm' model that describes the coincidence of crustal strain and strong focused erosion as the key element between surface and tectonic processes (Zeitler et al., 2001a). Significant amounts of erosion lead to heat advection and weakening of the crust, localization and intensification of strain, and building of high relief, which feeds back into continued rapid erosion. Alternatively, the locus of rapid exhumation (red region, Fig. 3) might have migrated towards the north through time with exhumation rates increasing through time. Discriminating between these two models would require data from other higher-temperature thermochronometers, taken from bedrock sampling across the entire NB antiform, on par with what has been collected for the NB-GP massif (e.g. Burg et al., 1998; Booth et al., 2004, 2009; Seward and Burg, 2008; Stewart et al., 2008)

Third, this study confirms exceptionally rapid modern denudation in the NB-GP antiform and massif. Zircon FT and related higher-temperature cooling ages of less than 1-2 Ma are generally rare worldwide. They are documented in the Himalaya including the syntaxial regions of the NB-GP massif and the Nanga Parbat massif (e.g. Cerveny et al., 1988; Zeitler et al., 2001b; Stewart et al., 2008) as well as in non-syntaxial areas of central Nepal and NW India (Blythe et al., 2007; Jain et al., 2000; Vannay et al., 2004; Bojar et al., 2005). In Alaska they are confined to a small area in the syntaxis region of the St. Elias Range (Enkelmann et al, 2009, 2010), and they have been reported from a few bedrock and detrital samples of the South Island of New Zealand (e.g. Herman et al., 2009; R.J. Stewart, pers. communication), and Taiwan (Willet et al., 2003; Kirstein et al., 2010).

The exhumation rate for the NB-GP antiform was computed using an annual sediment load measurement at Pasighat, which is likely to be quite uncertain and heavily influenced by the stochastic nature of monsoonal precipitation in the region; it may not be representative of longer time scale denudation rates in the region. For example, we estimate a modern denudation rate of 10 ± 5 mm/yr, which would correspond to exhumation magnitudes of 10-75 km over the last 2-5 Myr. We also used a 1D transient model to computed long-term exhumation rates. We estimated rates of 8 ± 1 mm/yr for the last 2 Myr. Previous estimates of long-term exhumation rates in the antiform range mostly from 3 to 5 mm/yr over the last ~5

Myr (e.g. Burg et al., 1998, Seward and Burg, 2008), however petrological studies also suggest rates of about 20 mm/yr that accommodated exhumation of mid-crustal rocks and decompressional melting (Booth et al., 2009). Although exhumation rates of up to 5 mm/yr are comparable to those documented by apatite thermochronometry elsewhere across the Himalayan Front (Greater Himalayan Sequence) in Nepal and NW India (e.g., Herman et al., 2010; Thiede et al., 2009; Huntington et al. 2006; Whipp and Ehlers, 2007; Whipp et al., 2007), they are exceptional with respect to (1) their amount of exhumation and persistence that is only revealed by the higher closure temperature systems (>200°C); and (2) the extensive region, ~5,000 km^2, they represent.

Acknowledgements:

We thank our collaborators of the Indentor corner project, particularly B. Hagedorn and D. Montgomery, for help during fieldwork and fruitful discussions. E. Enkelmann is grateful to J. Garver for the use of the fission track lab at Union College, and to R. Jonckheere for helpful discussion. We are thankful to the U.S. D.O.E. reactor use-sharing program (University of Oregon) for fission track irradiation, and to the Quaternary Research Center (University of Washington) for organizing and sponsoring the research expedition that enabled the samples collection. This manuscript was improved by constructive reviews by P. van der Beek and an anonymous reviewer. Data collection and analysis were supported by a grant from the Continental Dynamics Program of the U.S. National Science Foundation (grants 0003462 and 0003561).

Figure Captions:

Figure 1: Geological sketch of the eastern Himalaya with main geological units, structures, the Brahmaputra river system, and location of the detrital samples in this study. Inlet map shows the topography of the eastern part of the Himalaya - Tibetan region with the main rivers systems including the entire drainage of the Brahmaputra River.

Figure 2: Topographic map of the study area with published bedrock thermochronological ages. Zircon U-Th/He ages are from Stewart et al., 2008, zircon fission track (FT) ages from Burg et al., 1998; Seward and Burg, 2008, Biotite $^{40}Ar/^{39}Ar$ ages from Stewart et al., 2008, Zhang et al., 2004. Red and yellow lines outline the area with young (<2 Ma) zircon U-Th/He and biotite $^{40}Ar/^{39}Ar$ ages, respectively (after Stewart et al., 2008). ITS: Indus Tsangpo Suture; NB: Namche Barwa; GP: Gyala Peri.

Figure 3: Topography of the study area with sample locations and outlined drainage basins. Blue dots: detrital sample from the Brahmaputra River with age population shown on left. Red dots: detrital sample from tributaries with age population shown at the top of figure. Pie chart of the age population (P1-P8) and their percentage size of the entire grain distribution. Age populations with sizes ≤5% are not shown. n: is the number of measured grains per sample. Red contour line is the suggested extension of the region with <2 Ma zFT cooling ages based on the new detrital data of this study.

Figure 4: Probability density plot of the measured (black line) and peak fitted (grey line) zFT age distributions. Samples are arranged downstream starting from the top.

Figure 5: Estimated long-term denudation rates for locations in the Namche Barwa antiform (left) and the areas to the north and south (right) using a 1D transient thermal model. The 1 sigma error bars on the time are presented on the x-axis, and for the denudation rate on the y-axis.

REFERENCES:

Blythe, A.E., Burbank, D.W., Carter, A., Schmidt, K., Putkonen, J. 2007. Plio-Quaternary exhumation history of the central Nepalese Himalaya: 1. Apatite and zircon fission track and apatite [U-Th]/He analyses. Tectonics 26, TC3002, doi:10.1029/2006TC001990.

Bojar, A. V., Fritz, H., Nicolescu, S., Bregar, M. & Gupta, R. P. 2005. Timing and mechanisms of Central Himalayan exhumation: discriminating between tectonic and erosion processes. *Terra Nova* **17**, 427-433.

Booth, A.L., Zeitler, P.K., Kidd, W.S.F., Wooden, J., Liu, Y., Idleman, B., Hren, M., and Chamberlain, C.P., 2004, U-Pb zircon constraints on the tectonic evolution of southeastern Tibet, Namche Barwa Area: American Journal of Science, 304, p. 889–929, doi: 10.2475/ajs.304.10.889.

Booth, A.L., Chamberlain, C.P., Kidd, W.S.F., Zeitler, P.K. 2009. Constraints on the metamorphic evolution of the eastern Himalayan syntaxis from geochronologic and petrologic studies of Namche Barwa. GSA Bulletin 121, 385-407.

Brandon, M.T., 1992, Decomposition of fission-track grain-age distributions: American Journal of Science, v. 292, p. 535–564.

Brandon, M.T., 1996, Probability density plot for fission track grain-age samples: Radiation Measurements, v. 26, p. 663–676.

Brandon, M.T., Roden-Tice, M.K., and Garver, J.I., 1998, Late Cenozoic exhumation of the Cascadia accretionary wedge in the Olympic Mountains, northwest Washington State: Geological Society of America Bulletin, v. 110, p. 985–1009.

Burg, J.P., Nievergelt, P., Oberli, F., Seward, D., Davy, P., Maurin, J.-C., Diao, Z., and Meier, M., 1998, The Namche-Barwa syntaxis: Evidence for Exhumation related to compressional crustal folding: Journal of Asian Earth Sciences, v. 16, p. 239–252.

Carlson, W.D., Donelick, R.A., and Ketcham, R.A., 1999, Variability of apatite fission track annealing kinetics: I. Experimental Results: American Mineralogist, v. 84, p. 1213-1223.

Cerveny P.F., Naeser, N.D., Zeitler, P.K., Naeser, C.W., Johnson, N.M. 1988. History of Uplift and Relief of the Himalaya During the Past 18 Million Years: Evidence form Fission Track Ages of Detrital Zircons from Sandstones of the Siwalik Group. In: Frontiers in Sedimentary Geology, New Perspectives in Basin Analysis. K.L. Kleinspehn and C. Paola (edts.), Springer Verlag New York.

Cina, S. E., Yin, A., Grove, M., Dubey, C.S., Shukla, D.P., Lovera, O.M., Kelty, T.K., Gehrels, G.E., Foster, D.A., 2009. Gangdese arc detritus within the eastern Himalayan Neogene foreland basin: Implications for the Neogene evolution of the Yalu–Brahmaputra River system. Earth and Planetary Sciences Letters, 285, 150-162

Craw, D., Koons, P.O., Zeitler, P.K., and Kidd, W.S.F., 2005. Fluid evolution and thermal structure in the rapidly exhuming gneiss complex of Namche Barwa–Gyala Peri, eastern Himalayan syntaxis. Journal of Metamorphic Geology, 23, 829-845.

Ding, L., Zhong, D., Yin, A., Kapp, P., Harrison, T.M., 2001. Cenozoic structural and metamorphic evolution of the eastern Himalayan syntaxis (Namche Barwa). Earth and Planetary Science Letters 192 (3), 423–438.

Enkelmann, E., Zeitler, P.K., Garver, J.I., Pavlis, T.L., Hooks, B.P. 2010. The thermochronological record of tectonic and surface process interaction at the Yakutat–North American collision zone in southeast Alaska. *American Journal of Science* 310, 231-260.

Enkelmann, E., Zeitler, P.K., Pavlis, T.L, Garver, J.I., Ridgway, K.D. 2009. Intense localized rock uplift and erosion in the St Elias orogen of Alaska. Nature Geoscience 2, 5, 360-363.

Jain, A. K., Kumar, D., Singh, S., Kumar, A. & Lal, N. 2000.Timing, quantification and tectonic modelling of Pliocene- Quaternary movements in the NW Himalaya: evidence from fission track dating. *Earth Planet. Sci. Lett.* **179**, 437-451.

Todd A. Ehlers 2005. Crustal thermal processes and the interpretation of thermochronometer data. Reviews in Mineralogy and Petrology, vol. 58, p. 315-350.

Todd A. Ehlers, Tehmasp Chaudhri, Santosh Kumar, Chris W. Fuller, Sean D. Willett, Richard A. Ketcham, Mark T. Brandon, David X. Belton, Barry P. Kohn, Andrew J.W. Gleadow, Tibor J. Dunai, Frank Q. Fu 2005. Computational tools for low-temperature thermochronometer interpretation. Reviews in Mineralogy and Petrology, vol. 58, 589-622.

Farley, K.A. 2000. Helium diffusion from apatite: General behavior as illustrated by Durango fluorapatite. Journal of Geophysical Research, 105, B3, 293-2914.

Finlayson, D.P., Montgomery, D.R., Hallet, B., 2002. Spatial coincidence of rapid inferred erosion with young metamorphic massifs in the Himalayas. Geology, 30, 219-222.

Finnagen, N.J., Hallet, B., Montgomery, D.R., Zeitler, P.K., Stone, J.O., Anders, A.M., Yuping, L., 2008, Coupling of rock uplift and river incision in the Namche Barwa–Gyala Peri massif, Tibet. GSA Bulletin v. 120, p.142-155.

Galbraith, R.F., and Green, P.F., 1990, Estimating the component ages in a finite mixture: Nuclear Tracks and Radiation Measurements, v. 17, p. 197–206.

Garver, J. I. & Kamp, P. J. J. 2002. Integration of zircon color and zircon fission-track zonation patterns in orogenic belts: application to the Southern Alps, New Zealand. *Tectonophysics*, 349, 203-219.

Garver, J. I. 2003. Etching zircon age standards for fission-track analysis. *Rad. Meas*. 37, 47-53.

Garzanti, E., Vezzoli, G., Ando, S., France-Lanord, C., Singh, S.K., Foster, G., 2004. Sand petrology and focused erosion in collision orogens: the Brahmaputra case. Earth and Planetary Science Letters 220 (1–2), 157–174.

Goswami, D.C., 1985, Brahmaputra River, Assam, India: Physiography, basin denudation, and channel aggradation: Water Resources Research, v. 21, p. 959–978, doi: 10.1029/WR021i007p00959.

Green, P.F., Duddy, I.R., Gleadow, A.J.W., Tingate, P.T., Laslett, G.M. 1986, Thermal annealing of fission tracks in apatite: 1 - a qualitative description: Isotopic Geoscience v. 59, p. 237-253.

Hallet, B., and Molnar, P., 2001, Distorted drainage basins as markers of crustal strain east of the Himalaya: Journal of Geophysical Research, v. 106, p. 13,697–13,709, doi: 10.1029/2000JB900335.

Herman F., S.C. Cox and P.J.J. Kamp, 2009. Low-temperature thermochronology and thermokinematic modeling of deformation, exhumation, and development of topography in the central Southern Alps, New Zealand. Tectonics, 28: TC5011, doi:10.1029/2008TC00236#

Herman F., P. Copeland, J-P. Avouac, L. Bollinger, G. Mahéo, P. Le Fort, S. Rai, D. Foster, A. Pecher, K. Stuwe, P. Henry 2010. Exhumation, crustal deformation and thermal structure of the Nepal Himalaya derived from the inversion of thermochronological and thermobarometric data and modeling of the topography. Journal of Geophysical Research, Solid Earth, 115, B06407, doi:10.1029/2008JB006126.

Huntington, K.W., Blythe, A.E., Hodges, K.V. 2006. Climate change and Late Pliocene acceleration of erosion in the Himalaya. Earth and Planetary Science Letters 252, 107-118.

Kirstein, Fellin, M.G., Willett, S. D., Carter, A., Chen, Y-G, Garver, J. I., Lee, D. C., 2010. Pliocene onset of rapid exhumation inTaiwan during Arc-continent collision: new insights from detrital thermochronometry. Basin Research 22, 270–285, doi: 10.1111/j.1365-2117.2009.00426.x

Koons, P.O. 1995. Modeling the topographic evolution of collisional belts, Annual Review of Earth and Planetary Sciences, 23, 375-408.

Mancktelow, N.S., Graseman, B., 1997, Time-dependent effects of heat advection and topography on cooling histories during erosion: Tectonophysics, v. 270, p. 167-195.

McDougall, I. and Harrison, T.M. 1999. Geochronology and Thermochronology by the 40Ar/39Ar method, Oxford University Press pp. 267.

Rahl, J.M., Ehlers, T.A., van der Pluijm B.A., 2007, Quantifying transient erosion of orogens with detrital thermochronology from syntectonic basin deposits, *Earth and Planetary Science Letters*, v. 256, p. 147-161.

Rahn, M. K., Brandon, M. T., Batt, G. E., Garver, J. I., 2004. A zero-damage model for fission-track annealing in zircon. American Mineralogist 89, 473-484.

Reiners, P.W., Spell, T.L., Nicolescu, S., and Zanetti, K.A., 2004, Zircon (U-Th)/He thermochronometry: He diffusion and comparison with 40Ar/39Ar dating: Geochimica et Cosmochimica Acta, v. 68, p. 1857-1887.

Saddler, P.M., 1981, Sediment accumulation rates and the completeness of stratigraphic sections. Journal of Geology, 89, p. 569-584.

Schuster, D.L., Flowers, R.M., and Farley, K.A., 2006, The influence of natural radiation damage on helium diffusion kinetics in apatite: Earth and Planetary Science Letters, v. 249, p. 148-161.

Seward, D. and Burg, J.-P., 2008, Growth of the Namche Barwa Syntaxis and associated evolution of the Tsangpo Gorge: Constraints from structural and thermochronological data. Tectonophysics, 451, 282-289.

Singh, S.K., France-Lanord, C., 2002. Tracing the distribution of erosion in the Brahmaputra watershed from isotopic compositions of stream sediments. Earth and Planetary Science Letters 202 (3–4), 645–662.

Stewart, R.J., Hallet, B., Zeitler, P.K., Malloy, M.A., Allen C.M., Trippett, D. 2008. Brahmaputra sediment flux dominated by highly localized rapid erosion from the easternmost Himalaya. Geology 36;711-714.

Tagami, T. Galbraith, R. F. Yamada, R. Laslett, G. M. 1998, Revised annealing kinetics of fission tracks in zircon and geological implications. In *Advances in Fission-Track Geochronolgy,* P. Van den haute, F. De Corte, Eds. (Kluwer Acad. Publ.) pp. 99-112.

Thiede, R.C., Ehlers, T.A., Bookhagen, B., Strecker, M.R., 2009. Erosional variability along the northwestern Himalaya. Journal of Geophysical Research 114, F01015, doi:10.1029/2008JF001010

Tibari, B., Pik, R., France-Lanord, C. Carnigan, J., and Lave, J., 2005, Extreme uplift and erosion rates in eastern Himalayas (Siang-Brahmaputra Basin) revealed by detrital (U-Th)/He thermochronology (abstract): *Eos Trans AGU*, 86(52), T23C-0574.)

Vannay, J. C Grasemann, B., Rahn, M., Frank,W., Carter, A., Baudraz, V., Cosca, M. 2004.Miocene to Holocene exhumation of metamorphic crustal wedges in the Himalayan orogen: Evidence for tectonic extrusion coupled to fluvial erosion. *Tectonics* **23**, TC1014 doi:10.1029/2002TC001429, 2004

Whipp, D.M., Ehlers, T.A., 2007. Influence of groundwater flow on thermochronometer derived exhumation rates in the Nepalese Himalaya, *Geology* v. 35, p. 851-854

Whipp, D.M., Ehlers, T.A., Blythe, A., Ruhl, K., Hodges, K., Burbank, D., 2007, Plio-Quaternary erosion and kinematic history of the Central Himalaya: thermo-kinematic model of thermochronometer exhumation, *Tectonics,* v. 26, TC3003, doi:10.1029/2006/TC001991.

Whipp, D.M. Jr., Ehlers, T.A., Braun, J., Spath, C.D., 2009, Effects of exhumation kinematics and topographic evolution on detrital thermochronometer data, *J. Geophysical Res. – Earth Surface*, V. 114, F04014, doi:10.1029/2008JF001195

Willenbring, J. K. & von Blankenburg, F. 2010. Long-term stability of global erosion rates and weathering during late-Cenozoic cooling. Nature 465, 211-214. doi:10.1038/nature09044

Willet, S.D., Fisher, D., Fuller, C., Yeh, E., Lu, C., 2003. Erosion rates and orogenic wedge kinematics in Taiwan inferred from fission track thermochronometry. Geology, 31, 11, 945-948.

Yin, A., Harrison, T.M., 2000. Geological evolution of the Himalayan–Tibetan orogen. Annual Review of Earth and Planetary Sciences 28, 211– 280.

Zeitler, P.K., Meltzer, A.S., Koons, P.O., Craw, D., Hallet, B., Chamberlain, C.P., Kidd,W.S.F., Park, S.K., Seeber, L., Bishop, M., Shroder, J., 2001a. Erosion, Himalayan geodynamics, and the geomorphology of metamorphism. GSA Today 11 (1), 4–9.

Zeitler, P. K. and 19 others. 2001b. Crustal reworking at Nanga Parbat, Pakistan: Metamorphic consequences of thermal-mechanical coupling facilitated by erosion. Tectonics 20, 712-728.

Zhang, J., Ji, J., Zhong, D., Ding, L., He, S., 2004.Structural pattern of eastern Himalayan syntaxis in Namjagbarwa and ist formation process. Science in China Ser. D Earth Sciences. 47, no.2, 138-

Table 1: Summary of the sample location, detrital zFT results and peak fitting.

sample	Latitude N	Longitude E	Basin [km^2]	N	Age range	P1	P2	P3	P4	P5	P6	P7	P8	P9
Chinese tributaries														
*A**	-	-	4380	42	10-68					16±0.9 [75]			52±6.5 [25]	
B	29°54.940	95°37.748	4205	102	7-120				12±1.7 [25]	18±1.5 [48]		38±2.1 [25]		100±17 [2]
C*	-	-		45	3-28			6.7±0.4 [58]	12±1.2 [29]		24±2.3 [13]			
D	30°08.496	95°00.280	11520	103	0.9-53		3.8±0.5 [15]		10±0.6 [61]	17±1.8 [16]		37±3 [8]		
E	30°05.829	95°03.884		92	0.8-97		2.8±0.5 [10]		11±0.5 [34]		22±1.5 [23]	39±3.7 [23]	66±8.5 [10]	
F*	-	-	1531	50	2 -19		3.5±0.3 [61]	6.9±0.9 [22]		16±1.1 [17]				
G	29°52.180	93°39.816	4132	51	11-64				12±3.1 [6]			35±2.2 [62]	55±4.9 [32]	
H**	29°36.385	94°56.212	12	81	0.1-3.6	0.3 [35], 1.1 [34]	1.8 [26], 3.2 [5]							
Indian tributaries														
I	28°57.700	94°51.826	780	102	0.6-11	1.6±0.3 [27]	3.4±0.3 [69]		9±1.8 [4]					
J	28°54.599	94°46.441	159	103	1.4-25		4.6±0.5 [59]	7.2±1.2 [35]		17±3 [6]				
K	28°58.700	94°54.283	1290	101	8-66				13±0.9 [37]		20±1.3 [39]	34±2 [24]		
L	28°20.184	94°57.460	549	102	9-56					19±1.3 [46]	26±3.8 [39]	36±5.2 [15]		
M	28°13.187	94°51.321	4120	103	5-22			7.0±1 [18]	11±0.9 [61]	16±1.2 [21]				
N	28°11.099	95°13.211	1255	103	5-389					16±0.7 [84]	26±3 [12]			229±33 [4]
Brahmaputra River														
O*	-	-		50	6-99			7.5±0.5 [30]		17±1.2 [29]		40±2.7 [41]		
P	29°36.442	94°56.189		70	0.3-95	0.9±0.1 [27]			12±1 [28]			30±2.2 [40]	63±15 [5]	
Q	29°02.963	94°54.610		104	0.2-96	0.6±0.1 [48]	2.8±0.3 [21]		10±1 [15]	19±1.8 [11]			58±6 [5]	
R	28°34.628	95°04.222		103	0.2-78	1.1±0.1 [70]			11±0.6 [25]				45±4.3 [5]	
S	28°05.982	95°17.631	260000	108	0.2-56	0.9±0.1 [61]		7.3±0.5 [21]		19±1.2 [16]			49±7 [2]	
301*				101	0.1-50	0,6±0.1 [47]	4.7±0.4 [13]		10±0.8 [17]	18±1.3 [21]		37±7 [2]		

Note: N is number of measured single grain ages; P is peak age in Ma ±1sigma of the deconvolved age populations using Binomfit peak fitting of M. Brandon, in brackets is the size of age population in %; samples noted with* are published in Steward et al., 2008; sample NB904** is a unpublished sample analyzed by W. Stewart

***Highlights**

Research highlights:

- The rapidly exhuming Namche Barwa massif is a major source of sediments to the Tsangpo-Siang River system, composing 60-70% of the entire sediment load
- New detrital zircon cooling ages reveal exhumation rates of 7 -12 mm/yr at the Namche Barwa antiform.
- Region of rapid and localized exhumation in the Namche Barwa massif extends ca. 50 km further southwest than previously recognized

Figure 1
Click here to download high resolution image

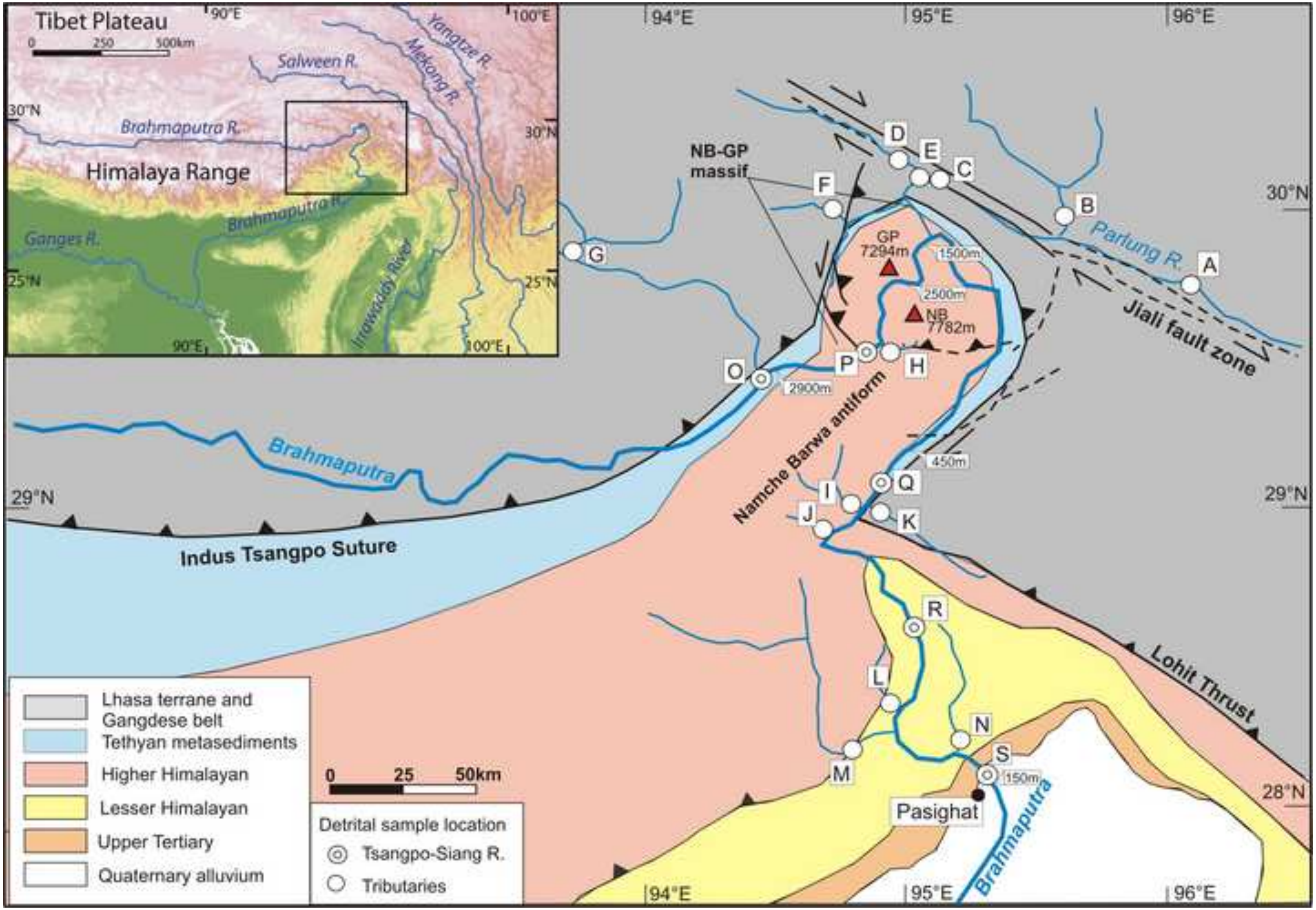

Figure 2
Click here to download high resolution image

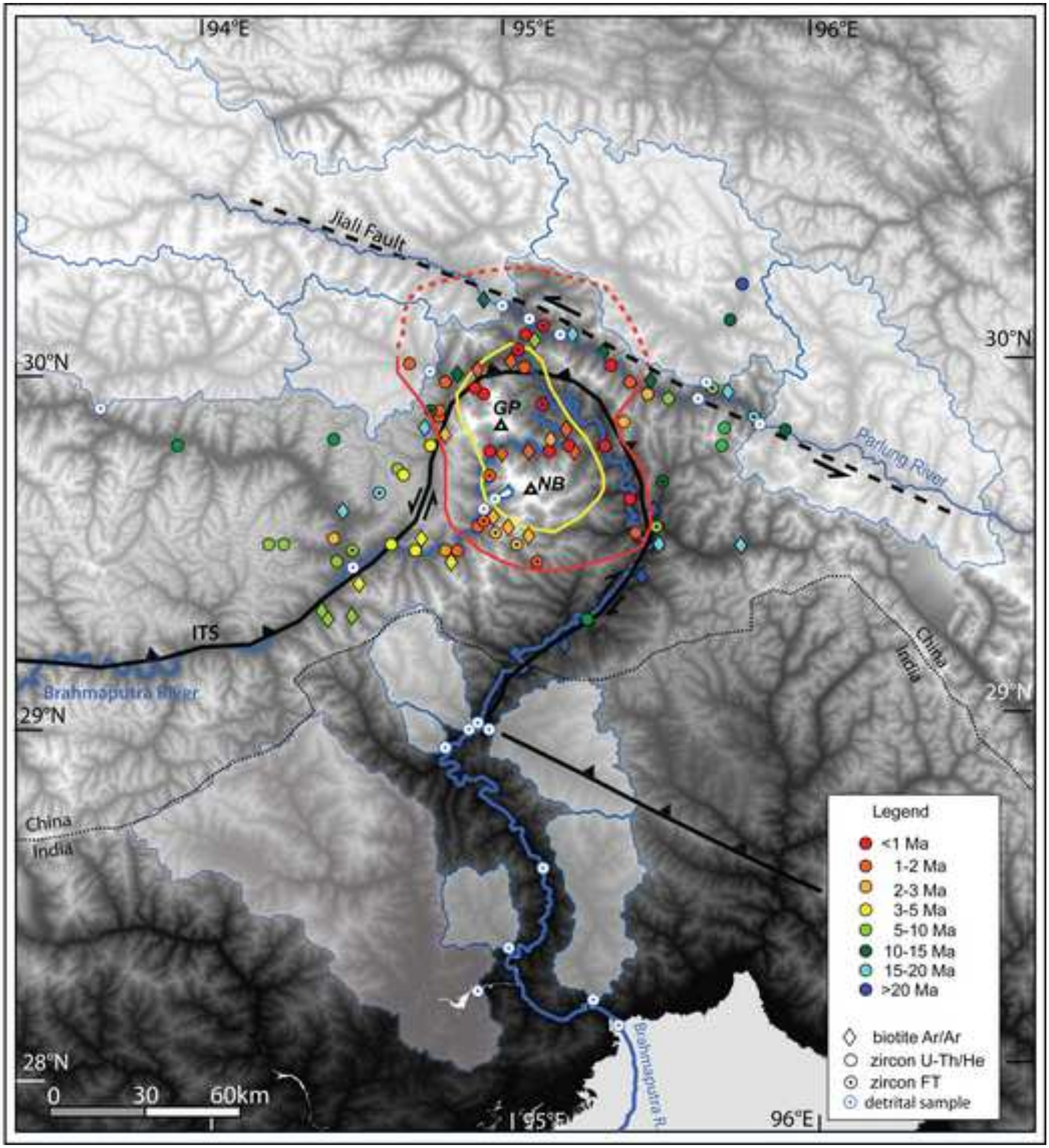

Figure 3
Click here to download high resolution image

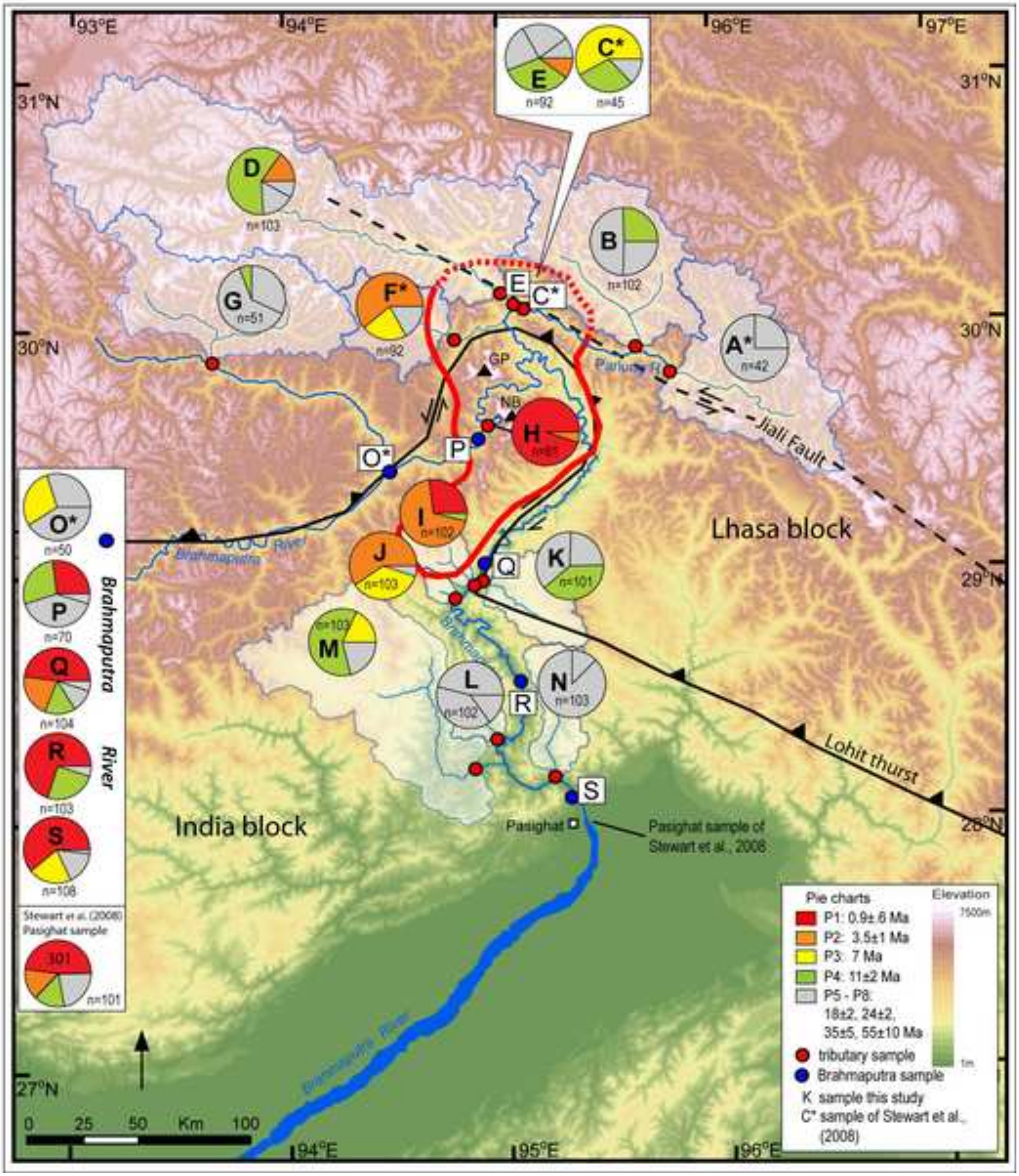

Figure 4
Click here to download high resolution image

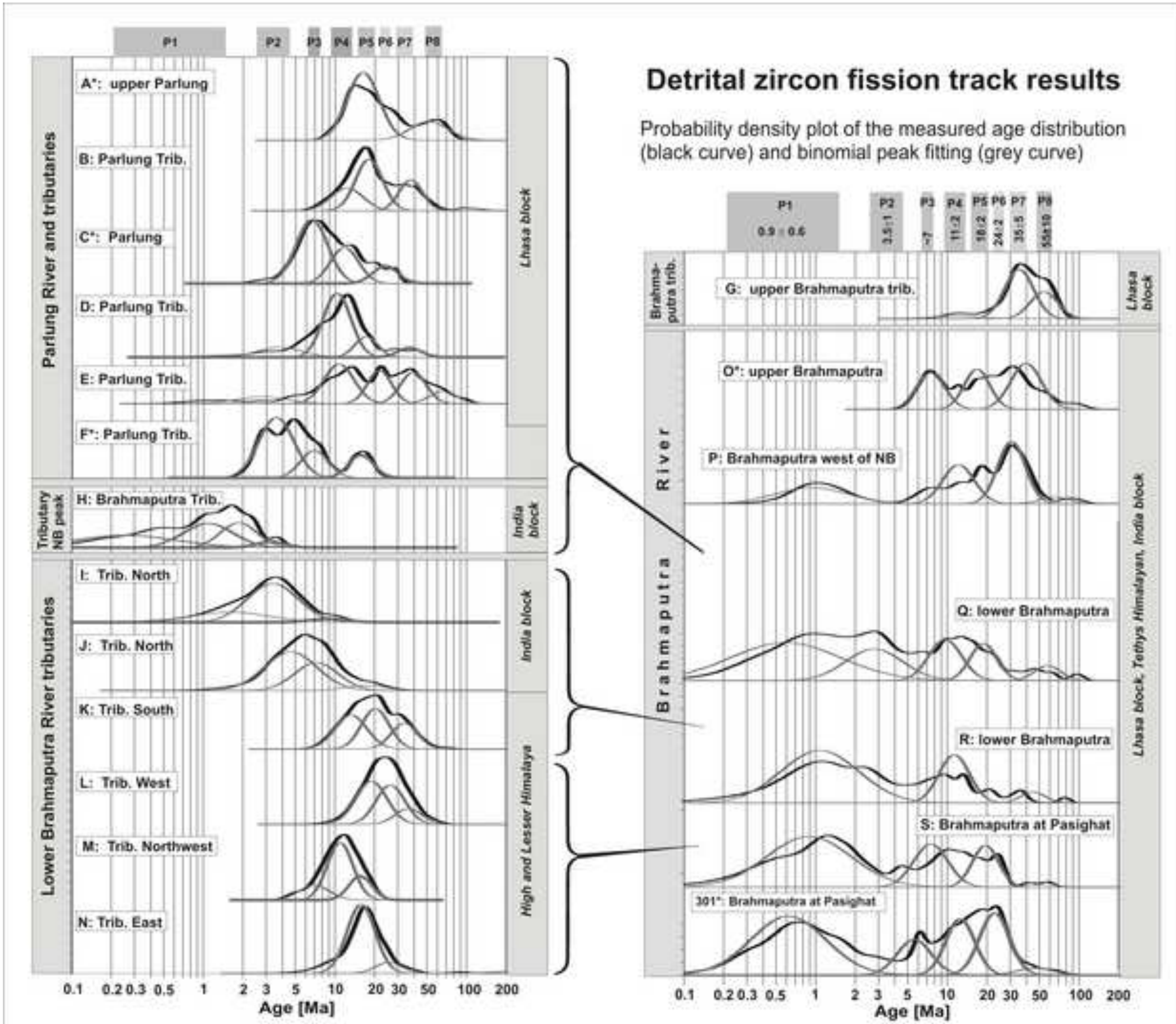

Figure 5

Click here to download high resolution image